

## Radiation trapping in sodium—noble-gas mixtures

J. Huennekens, H. J. Park,\* T. Colbert, and S. C. McClain†  
*Department of Physics, Lehigh University, Bethlehem, Pennsylvania 18015*  
 (Received 15 October 1986)

We have studied sodium resonance radiation under conditions of severe radiation trapping in sodium-argon mixtures, and we report measured values of the effective radiative decay rates. The measured values are compared with values calculated from the Holstein theory of radiation trapping in the impact-regime, foreign-gas pressure-broadening limit. The experiment was designed to satisfy all of the validity criteria imposed by the approximations of the Holstein theory, and the experiment and theory are in good agreement. Since the effective radiative decay rate depends upon the collisional line-broadening rate, confirmation of the theory allows such measurements to be used to determine unknown line-broadening constants using only broadband lasers and low resolution monochrometers. We demonstrate this technique for the sodium *D* lines broadened by xenon and neon perturbers. The values for the broadening constants obtained in this manner are in reasonable agreement with values from several previous studies utilizing more traditional techniques.

### I. INTRODUCTION

In an optically thick vapor, resonance photons may be absorbed and reemitted many times before they escape to the container walls. This process, called radiation trapping, must be understood in order to accurately model stellar atmospheres<sup>1</sup> and to correctly interpret studies of atomic collisions in optically thick vapors.<sup>2,3</sup> Additionally, radiation trapping is important in the lighting industry since it is a process which reduces the efficiency of commercial lamps.<sup>4,5</sup>

Trapping of resonance radiation can be expressed in terms of the escape factor  $g$  which relates the effective radiative rate to the natural radiative rate:<sup>6,7</sup>

$$\Gamma_{\text{eff}} = g \Gamma_{\text{nat}}. \quad (1)$$

Thus  $g^{-1}$  can be thought of as the mean number of absorptions and reemissions that take place before escape. The escape factor depends on the line-center optical depth, the magnitudes and types of line-broadening mechanisms that are active, and the geometry of the cell.

In principle, very accurate results for the escape factor can be obtained using Monte Carlo techniques if one knows the distribution of absorbing atoms (usually ground-state atoms), the line-shape function  $k_\nu$ , the frequency and angular redistribution functions, and any relevant collisional excitation transfer rates. In practice, excellent results have been obtained using these techniques which can handle such complications as hyperfine structure and nonideal geometries.<sup>5</sup> However, such computer simulations are expensive and it is not obvious how to scale the results if, for instance, one doubles the cell size or changes the type of either the radiating or perturbing atoms.

By employing certain approximations and considering limiting cases, Holstein obtained simple analytic expressions for the escape factor which are valid under a wide range of conditions.<sup>6,7</sup> In particular, Holstein used the limiting approximations of high optical depth ( $k_0 L \gg 1$ ,

where  $k_0$  is the line-center absorption coefficient and  $L$  is the cell dimension), only a single broadening mechanism present (pure Doppler, pure impact-regime collision broadening, or pure quasistatic-regime collision broadening), and complete frequency redistribution. He then considered ideal geometries (infinite slab and infinite cylinder) and wrote the solutions to the radiation diffusion equation for the excited-atom spatial distribution as an eigenmode expansion,

$$n_e(\mathbf{r}, t) = \sum_i C_i n_i(\mathbf{r}) e^{-\beta_i t}. \quad (2)$$

The spatial modes  $n_i(\mathbf{r})$  form a complete set of functions, each mode being a solution to the radiation diffusion equation that decays exponentially. In general, the excited-atom spatial distribution will not decay as a single exponential but will evolve in time toward the fundamental (i.e., slowest decaying) mode distribution  $n_1(\mathbf{r})$ . Note that except for the fundamental mode, the spatial modes are nonphysical since  $n_i(\mathbf{r})$  can be negative for  $i \neq 1$  (see Ref. 8 for plots of the four lowest spatial mode distributions). The total excited-atom density  $n_e(\mathbf{r}, t)$  must, of course, be positive everywhere.

Holstein solved for the fundamental mode decay rate  $\beta_1$  which is equal to  $\Gamma_{\text{eff}}$  in the limit of a fundamental mode distribution. For the geometry of an infinite slab of thickness  $L$  he obtained

$$\Gamma_{\text{eff}} = g \Gamma_{\text{nat}} = 1.875 \Gamma_{\text{nat}} \{k_0 L [\pi \ln(k_0 L / 2)]^{1/2}\}^{-1} \quad (3)$$

for a Doppler-broadened line, and

$$\Gamma_{\text{eff}} = g \Gamma_{\text{nat}} = 1.150 \Gamma_{\text{nat}} \left[ \frac{\lambda^2}{2} \frac{g_2}{g_1} L n \frac{\Gamma_{\text{nat}}}{\Gamma_c} \right]^{-1/2} \quad (4)$$

for a collision-broadened line in the impact regime. Here,  $\lambda$  is the transition wavelength,  $g_2$  and  $g_1$  are the upper and lower state statistical weights, and  $\Gamma_c$  is the collisional-broadening rate which has a contribution from

self-broadening and one from foreign-gas broadening, i.e.,

$$\Gamma_c = nk_c^{\text{self}} + n_p k_c^{\text{foreign}} \quad (5)$$

The  $k_c$ 's are collisional-broadening rate constants and  $n$  and  $n_p$  are the absorbing-radiating and perturbing atom densities, respectively.

Similar results for infinite cylinder geometries and for quasistatic-regime pressure broadening can be found in Holstein's papers.<sup>6,7</sup> van Trigt extended the calculations to obtain decay rates for several of the higher modes.<sup>8,9</sup>

In a previous work we experimentally verified the Holstein solutions for the escape factor in the pure self-broadening limit (pure Na vapor).<sup>10</sup> This required the use of experimental conditions which satisfy the approximations and limitations imposed by the theory. In the present work we extend these measurements to the foreign-gas broadening case (Na perturbed by Ar). Again, we find that the simple Holstein expressions yield escape factors and effective radiative rates that agree with our measured values within experimental uncertainties. Using this result, we demonstrate that simple measurements of effective radiative rates, using broadband lasers and low-resolution monochromators, can be used in some cases to obtain reasonably accurate values for unknown impact-regime line-broadening rates. We demonstrate the technique in the cases of Na perturbed by Xe and Ne.

## II. THE EXPERIMENT

In order to experimentally test the Holstein results, it is essential that the conditions of the experiment meet the validity criteria of the theory. In the present experiment, we study sodium perturbed by argon because the rates for broadening of the sodium resonance lines by argon are known accurately,<sup>11–15</sup> as are the sodium resonance line self-broadening rates.<sup>3</sup> The fine structure of the sodium  $3P$  state is a complication which must be accounted for

(see Sec. III), but the rate coefficients for excitation transfer between the two levels are also accurately known.<sup>3,16,17</sup> The rate coefficient for quenching of sodium  $3P$  atoms by argon is quite small ( $k_{\text{quench}} < 10^{-13}$  cm<sup>3</sup>/s),<sup>18</sup> and this process can be neglected here (see also Sec. III). Quenching by Na<sub>2</sub> molecules and impurities will be considered later.

The experimental setup is shown in Fig. 1. The commercial nitrogen laser pumps a home-built dye laser which produces 0.5-ns pulses of light in a 0.1–0.2-nm bandwidth around 589 nm. Typically, the laser energy is 10–15 μJ/pulse. The sodium cell is a stainless-steel block, drilled out to make a cross, which has sapphire windows sealed to the block with silver O rings. The cell is uniformly heated (including the windows) so that density gradients are minimized. The cell is connected to a vacuum and gas handling system, and the sodium vapor pressure is controlled by the temperature of a sidearm which is kept lower than the cell temperature to avoid Na condensation on the windows. Two arms of the cross contain sapphire rods which create a slab geometry in the observation region. Since the spacing between the rods, 0.537 cm, is small compared to their diameter, 1.27 cm, the observation region approximates Holstein's infinite slab. Fluorescence is collected by a lens system, dispersed by a 0.5-m monochromator and detected by a photomultiplier (PMT). The PMT output is amplified by a fast amplifier, passes down a 107-ft. delay line and is then processed by a boxcar averager with scannable gate. Boxcar signals are sent to a computer where 5 scans are averaged. The boxcar is triggered by a photodiode (PD) which observes a fraction of the laser pulse split off by a beam splitter. The time resolution for the complete system was measured to be ~12 ns. A white lamp on the far side of the cell is used to measure absorption equivalent widths from which sodium densities are determined.

We operate at sodium densities between  $5 \times 10^{12}$  cm<sup>-3</sup> and  $2 \times 10^{14}$  cm<sup>-3</sup>. This yields line-center optical depths

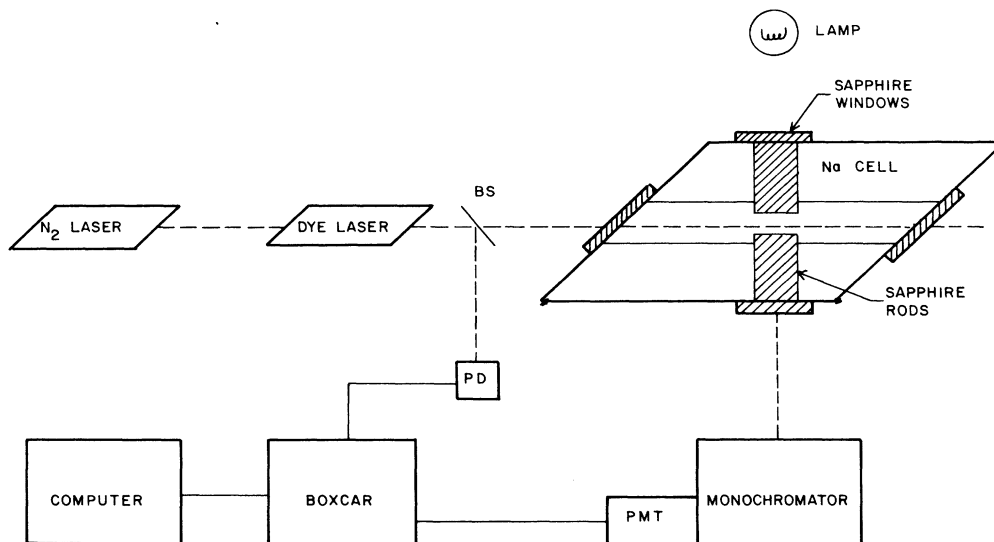


FIG. 1. Experimental setup.

(in the absence of argon gas) between 8 and 600, thus satisfying Holstein's requirement of high optical depth. The requirement of a single broadening mechanism is clearly not satisfied since Doppler, pressure, and natural broadening are all simultaneously present in the resonance lines. However, the radiation trapping problem is almost totally dominated by the part of the line profile where the optical depth is approximately unity (i.e.,  $k_\nu L \sim 1$ ). This is because photons emitted at frequencies closer to line center are absorbed after traveling a very short distance regardless of the details of the line shape, while there is only a small probability for emission at larger detunings from line center. This same effect is responsible for the fact that the peaks of a self-reversed line appear near the  $k_\nu L = 1$  points. Thus the dominant broadening mechanism with respect to radiation trapping is that which dominates the unity optical depth points of the line profile. Note that since the Lorentzian function has much more persistent wings than does the Gaussian function, pressure broadening can dominate radiation trapping at much lower densities than the point where the pressure-broadened half width equals the Doppler half width. We also note that the transition between Doppler- and pressure-broadened radiation trapping occurs quite suddenly (i.e., see the  $[\text{Na}] = 5.27 \times 10^{12} \text{ cm}^{-3}$  data of Fig. 4 and also Fig. 5 of Ref. 10). Thus the Holstein approximation of a single broadening mechanism is not a serious constraint. Note that the collision-induced line shift, which can be several Doppler widths at 1000 Torr of argon, does not affect the trapping as long as this shift is constant throughout the cell. Additionally, reabsorption of  $D_1$  line-wing photons in the optically thick regions of the  $D_2$  line and vice versa is negligible (less than a 1.5% effect on  $\Gamma_{\text{eff}}$ ).

The final approximation of the Holstein theory is the assumption of complete frequency redistribution; i.e., that the frequency of the emitted photon is not correlated to the frequency of the absorbed photon. This is a very good approximation for Doppler and pressure broadening, but is very poor for natural broadening (where there is no redistribution in the atom's rest frame). Under the conditions of our experiment, this is not a problem since in all cases where the Lorentzian wings dominate the radiation trapping problem, the contribution from pressure broadening exceeds the natural-broadening contribution. However, this does not have to be the case if  $\Gamma_{\text{nat}}$  is large, the Doppler width is small, or the cell dimensions are large. Recently Post *et al.*<sup>19,20</sup> and Streater<sup>21</sup> have carried out extensive tests of the effects of incomplete redistribution on radiation trapping. More will be said about this in Sec. III.

Since the Holstein theory yields fundamental mode decay rates, we must consider whether that is what we measure in the experiment. In general, the laser excites some linear combination of spatial modes [see Eq. (2)] which then decays as a sum of exponentials. Since the fundamental mode has the slowest decay, a pure fundamental mode can be achieved by simply waiting until the late time. [Note that the second slowest decaying symmetric mode,  $n_3(\mathbf{r})$ , which is the next most important for our experimental conditions, decays with a rate 2.09 times that

of the fundamental mode.<sup>8,9</sup>] For a typical scan (see Fig. 2) we fit a single exponential to the data beginning at some initial time  $t_0$ . We then repeat the fit using a larger value of  $t_0$  and continue until we find the decay rate converging toward a constant value. However, if not much care is taken with the excitation laser spatial profile, it may take a very long time to reach single exponential decay. On the other hand, we can minimize this effect by making a reasonable match between the laser spatial profile and the fundamental mode distribution [see Fig. 3(c)]. In this way we excite the fundamental mode with a large amplitude while the amplitudes of higher modes are small [ $C_1 > C_i$ ,  $i \neq 1$  in Eq. (2)]. Thus we reach a single exponential decay at fairly early times. Note that the radiation trapping process quickly washes out any inhomogeneities in the excited atom distribution caused by the poor laser spatial mode structure, etc., and only a crude match of beam diameter with the cell dimension is necessary.

The method of imaging of the fluorescence onto the detector can also affect the observed decay rates. Figures 3(a) and 3(b) show the cell geometry. The cell interior is imaged onto the monochromator entrance slits with the  $x$  axis oriented along the slits. Orienting the  $z$  axis along the slits increases signal size but fails to account for photons that diffuse out of the laser column. Thus the trapping geometry would be determined by the laser beam diameter and the monochromator slit width rather than by the slab thickness  $L$ . Since the excitation is approximately independent of  $z$  (attenuation across the observed region is small) it is more nearly correct to image a slice oriented along  $x$ . Then, by symmetry, the photons diffusing out of this volume into other region of the cell are compensated by an equal number diffusing in.

Neutral density filters were inserted into the fluorescence to test detector linearity, and into the laser beam to verify that nonlinear processes (for example, quenching by electrons created in associative ionization or photoioniza-

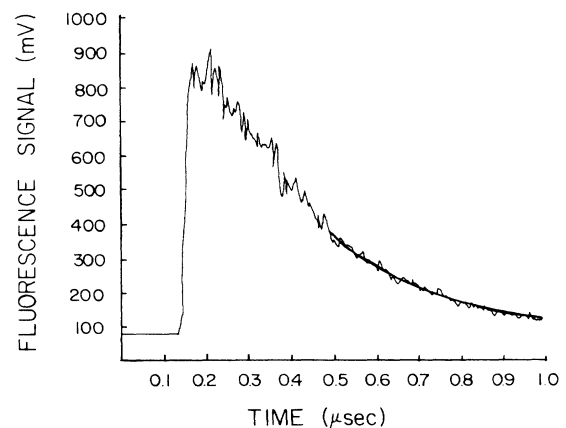


FIG. 2.  $D_2$  fluorescence intensity as a function of time (average of 5 scans). The laser, which was set to the  $D_2$  line frequency, fired at  $t \sim 0.14 \mu\text{sec}$ .  $[\text{Na}] = 1.14 \times 10^{14} \text{ cm}^{-3}$ . Argon pressure was 500 Torr. The smooth curve superimposed on the data is a fitted exponential.

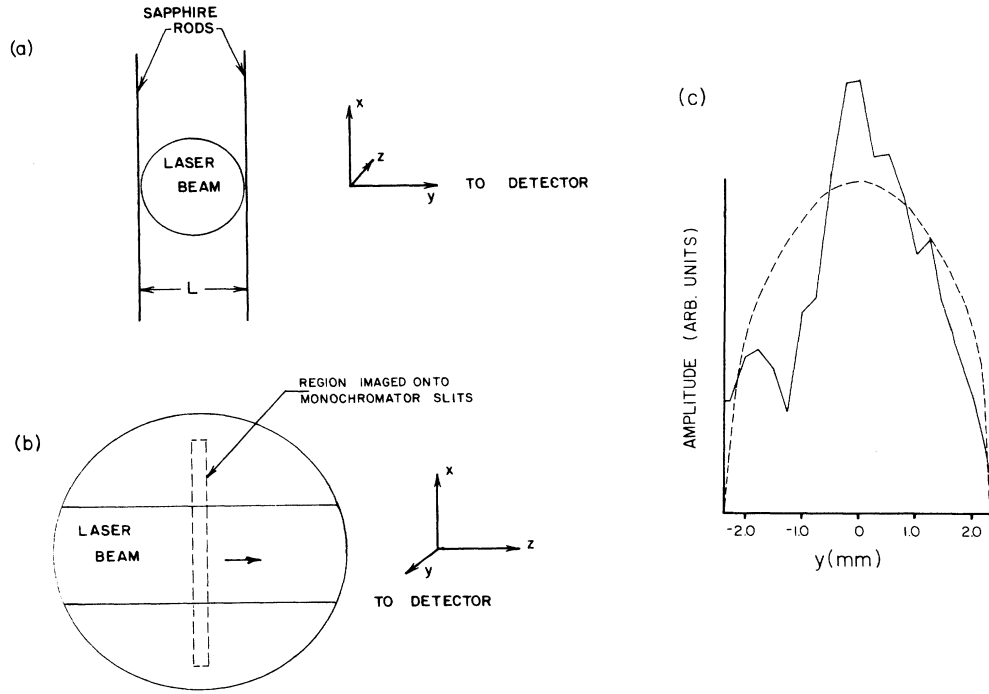


FIG. 3. (a) Cross section of the cell interior in the  $xy$  plane. The laser beam propagates into the page ( $z$  direction). (b) Cross section in the  $xz$  plane. This is the view which is seen from the detector. The dashed line indicates the region imaged onto the monochromator slits. (c) Comparison of the laser spatial profile (solid line) measured across the cell [in the  $y$  direction of (a) and (b)] and the fundamental-mode excited-atom spatial distribution (dashed line).

tion) did not modify the decay rates. Laser and monochromator bandwidths were such that the  $D_1$  and  $D_2$  lines could easily be resolved in both excitation and detection, although we will see that the rapid collisional excitation transfer between the two upper levels makes this resolution unnecessary.

### III. RESULTS AND DISCUSSION

Because of excitation transfer between the two levels, the observed decay rate is actually a mixture of the  $\Gamma_{\text{eff}}$ 's for the  $D_1$  and  $D_2$  lines. (These are unequal due to different statistical weights and collisional broadening rates for the  $3P_{1/2}$  and  $3P_{3/2}$  states.) If we label  $3P_{3/2}$  state 2 (the state directly excited by the laser) and  $3P_{1/2}$  state 1 then we find that the following rate equations are valid once the laser pulse has terminated:

$$\dot{n}_2 = R_{12}n_1 - (\Gamma_{2\text{eff}} + R_{21})n_2, \quad (6)$$

$$\dot{n}_1 = R_{21}n_2 - (\Gamma_{1\text{eff}} + R_{12})n_1. \quad (7)$$

Here the  $R$ 's are collisional mixing rates which have one contribution from collisions with ground-state sodium and one from collisions with perturbers

$$(R_{21} = k_{21}^{\text{Na}}n + k_{21}^p n_p).$$

The solution to Eqs. (6) and (7) is

$$n_2(t) = \frac{n_2(0)}{\omega_+ - \omega_-} [(\Gamma_{1\text{eff}} + R_{12} - \omega_-)e^{-\omega_- t} + (\omega_+ - \Gamma_{1\text{eff}} - R_{12})e^{-\omega_+ t}], \quad (8)$$

$$n_1(t) = \frac{n_2(0)}{\omega_+ - \omega_-} R_{21}(e^{-\omega_- t} - e^{-\omega_+ t}), \quad (9)$$

where  $n_2(0)$  is the initial population in the  $3P_{3/2}$  state produced by the laser and  $\omega_{\pm}$  are given by

$$\omega_{\pm} = \frac{1}{2}(\Gamma_{1\text{eff}} + \Gamma_{2\text{eff}} + R_{12} + R_{21}) \pm \frac{1}{2}[(\Gamma_{1\text{eff}} - \Gamma_{2\text{eff}})^2 + 2(R_{12} - R_{21})(\Gamma_{1\text{eff}} - \Gamma_{2\text{eff}}) + (R_{21} + R_{12})^2]^{1/2}. \quad (10)$$

In the limit of low collisional mixing,  $\omega_{\pm}$  reduce to  $\Gamma_{1\text{eff}}$  and  $\Gamma_{2\text{eff}}$ . However, for complete mixing (i.e.,  $R \gg \Gamma_{\text{eff}}$ ), we find  $\omega_+ \sim R_{21} + R_{12}$  while

$$\omega_- \sim \frac{1}{3}\Gamma_{1\text{eff}} + \frac{2}{3}\Gamma_{2\text{eff}}$$

(i.e.,  $\omega_-$  reduces to the weighted mean of the effective radiative rates assuming  $R_{12} \sim 2R_{21}$  from detailed balance. For our temperature of 630 K,  $R_{12} = 1.92R_{21}$  so  $\omega_- = 0.342\Gamma_{1\text{eff}} + 0.658\Gamma_{2\text{eff}}$  in the complete mixing limit.) If  $\omega_+ \gg \omega_-$ , the slow decay rate dominates the fluorescence decay in the late time and is therefore the

quantity measured in the experiment. In principle,  $\omega_+$  could be obtained from the fast exponential rise of the  $D_1$  fluorescence and thereby would yield the mixing rates. However, for even 1 Torr of argon this fast rise is much faster than the detection system response time.

Measurements of fluorescence decay rates for both  $D$  lines were taken as a function of argon pressure for four sodium densities. These results are plotted in Fig. 4 along with calculated fluorescence decay rates ( $\omega_-$ ) obtained from Eq. (10). The mixing rates were calculated from the results of Refs. 3 and 16 and the principle of detailed balance.  $\Gamma_{\text{eff}}$ 's were calculated from Eqs. (3) and (4) using  $k_0(D_2)/n = 5.63 \times 10^{-12} \text{ cm}^2$  and  $k_0(D_1)/n = 2.81 \times 10^{-12} \text{ cm}^2$  (which are corrected for the 1.77-GHz ground-state hyperfine splitting), self-broadening rates from Ref. 3, and argon broadening rates from the weighted mean of the results of Refs. 11–15 [ $k_c^{\text{Ar}}(D_2) = 4.87 \times 10^{-9} \text{ cm}^3 \text{ s}^{-1}$ ,  $k_c^{\text{Ar}}(D_1) = 5.38 \times 10^{-9} \text{ cm}^3 \text{ s}^{-1}$ ]. (Note that the argon broadening constants were scaled to our temperature of 630 K using the theoretical  $T^{0.3}$  temperature dependence appropriate for van der Waals broadening.<sup>22</sup>) Values of  $\Gamma_{\text{nat}}$  were taken from Ref. 23. The crossover from Doppler to pressure broadening (which only occurs for data taken at the lower Na densities) was handled by simply taking the larger of  $\Gamma_{\text{eff}}(\text{Doppler})$  and  $\Gamma_{\text{eff}}(\text{impact})$ .

Error bars have been placed on several points on the graph. One of the most significant sources of error is the uncertainty in the sodium density. This was obtained at each side arm temperature from Nesmayanov's vapor

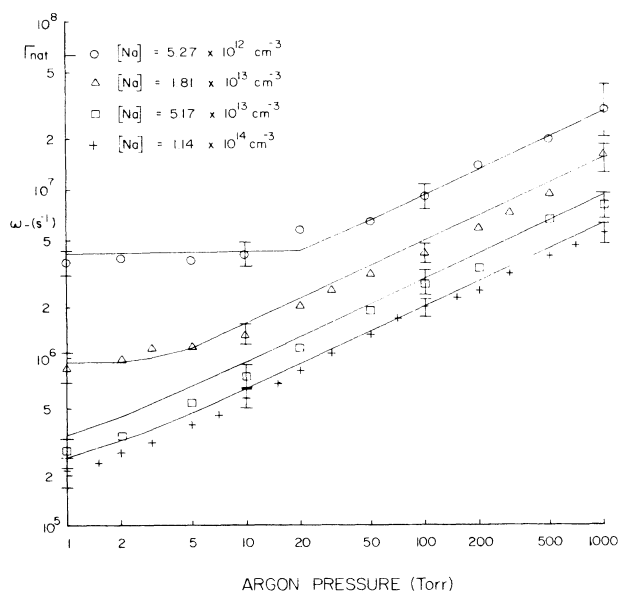


FIG. 4. Fluorescence decay rates  $\omega_-$  as a function of argon pressure for sodium densities of  $5.27 \times 10^{12}$ ,  $1.81 \times 10^{13}$ ,  $5.17 \times 10^{13}$ , and  $1.14 \times 10^{14} \text{ cm}^{-3}$ . Solid line is the Holstein theory prediction. The horizontal regions of the  $\omega_-$  versus pressure curves at the two lowest sodium densities are regions where the trapping is dominated by Doppler broadening (and is therefore independent of gas density).

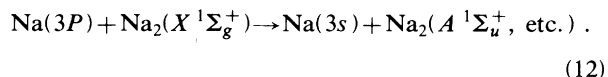
pressure formula<sup>24</sup> and from  $D$  line equivalent width measurements taken at several argon pressures and with no gas present. The pure sodium equivalent widths were compared to values calculated by Kunasz and Kamke<sup>25</sup> (which include hyperfine-structure effects) while the equivalent widths for argon broadening were calculated from the expression:<sup>22,26</sup>

$$W_\lambda = \frac{\lambda^2}{c} \left[ \frac{\lambda^2}{8\pi^2} \frac{g_2}{g_1} L n \Gamma_c \Gamma_{\text{nat}} \right]^{1/2}, \quad (11)$$

which is valid when the pressure broadened wings dominate the equivalent width (this is roughly the same criteria as when the pressure broadened wings dominate the radiation trapping; i.e., that the unity optical depth point is in the pressure-broadened wings). The various Na density determinations typically agree to within  $\sim 20\%$  and we estimate the uncertainty of their mean at  $\sim 10\%$ . The uncertainty in the argon pressure is very small (we take it to be less than 1% for  $P > 100$  Torr and less than 5% for  $10 < P < 100$  Torr). However, due to the coarse scales of the pressure gauges used, the uncertainty in the argon pressure is substantial ( $\sim 25\%$ ) in the range of 1–2 Torr. Nevertheless, this is not a serious concern at either low Na densities where the trapping is dominated by the Doppler core (for low Ar pressures) or at high Na densities where self-broadening exceeds the Ar broadening (for low Ar pressures).

Excitation transfer rates are known to  $\sim 18\%$  for sodium-sodium collisions<sup>3</sup> and  $\sim 5\%$  for sodium-argon collisions,<sup>16</sup> but for argon pressures above a few Torr the mixing is complete and we are totally insensitive to errors in the mixing rates. The sodium self-broadening rates are known to 15%,<sup>3</sup> while the rates for broadening by argon are known to  $\sim 5\%$ .<sup>11–15</sup> The measured decay rates were corrected for the 12-ns time resolution of the detection system. This correction represents a 36% increase in our largest  $\omega_-$  values obtained at low Na density, but this drops to less than 12% for  $\omega_- = 10^7 \text{ s}^{-1}$  and to less than 4% for  $\omega_- = 3 \times 10^6 \text{ s}^{-1}$ . As can be seen from Fig. 4, almost all of the data correspond to  $\omega_- < 10^7 \text{ s}^{-1}$ . In all cases, the entire magnitude of the correction was folded into the overall error estimate. The influence of higher spatial modes is greatly reduced by the pump beam geometry and the exponential fitting technique. We estimate that these higher modes contribute less than a 5% error in our results. Window reflectivity introduces a systematic error, since reflections back into the vapor increase the average photon escape time. Conversely, the window reflectivity can be thought of as an effective increase in the slab thickness. From our previous study of pure sodium vapor, and from the known reflectivity of the sapphire surfaces, we estimate an approximate error of 5% in our measured values of  $\omega_-$  from this cause. The data were not corrected for this effect. Finally, the statistical uncertainty of the data itself and of the fitting routine is estimated to be less than 5%. Assuming the various sources of uncertainty are uncorrelated, and taking account of the functional dependence of  $\Gamma_{\text{eff}}$  on the various parameters, we estimate that our experimentally determined decay rates ( $\omega_-$ ) are typically accurate to 10–20%.

Quenching collisions can increase observed decay rates which therefore do not correctly reflect the effective radiative rates. Quenching can occur in collisions of excited Na with Na<sub>2</sub> molecules, argon atoms, or impurity atoms and molecules which are present in the argon or which outgas from the cell walls. Na<sub>2</sub> molecules are efficient quenchers through the process:



The rate coefficient for this process was measured to be  $3.4 \times 10^{-9} \text{ cm}^3 \text{ s}^{-1}$  by Lam *et al.*<sup>27</sup> who observed an increase in the fluorescence decay rates when the Na density was greater than  $10^{15} \text{ cm}^{-3}$ . However, for our largest Na<sub>2</sub> density of  $1.07 \times 10^{11} \text{ cm}^{-3}$ ,<sup>28</sup> this quenching mechanism has less than a 0.2% effect on the observed decay rates.

Copley, Kibble, and Krause<sup>18</sup> showed that cross sections for quenching of sodium by noble gases are less than  $10^{-18} \text{ cm}^2$ . These results are also supported by shock tube measurements of Tsuchiya and Kuratani<sup>29</sup> and by calculations of Stamper.<sup>30</sup> Using  $10^{-18} \text{ cm}^2$  as an upper value we find that quenching by argon could affect our measured decay rates by 28% in the worst case (i.e., our  $n = 1.14 \times 10^{14} \text{ cm}^{-3}$ , 1000 Torr Ar point). However, quenching by argon would cause a linear dependence of  $\omega_-$  on argon pressure. Our observed square-root dependence also confirms  $10^{-18} \text{ cm}^2$  as an upper limit for the quenching cross section and demonstrates that argon quenching does not significantly affect our results.

Impurities in the argon, especially diatomic molecules, can be very efficient quenchers. For example, measured values of the cross section for quenching of Na(3P) by N<sub>2</sub> range from  $1 \times 10^{-15}$  to  $5 \times 10^{-15} \text{ cm}^2$ .<sup>29,31–34</sup> However, the argon used in the present experiment has a purity level of 99.998%. If we assume all impurities quench with an effective cross section of  $5 \times 10^{-15} \text{ cm}^2$ , we estimate that they cause less than a 3% increase in the observed decay rates. As with the quenching by the argon itself, quenching by impurities in the argon would cause a linear dependence of observed decay rates on argon pressure. Thus we conclude that these mechanisms also do not significantly affect our experiment.

Finally we note that after adding argon to the cell and sealing it off from the vacuum system, impurities produced by outgassing can build up with time and result in significant quenching. This effect would cause an increase in  $\omega_-$  with time following the closing of the cell valve. However, no noticeable change in  $\omega_-$  was recorded over a period of one hour, which was typical of the time the valve remained closed during the experiment.

Within the uncertainty of our measurements, we have confirmed the validity of the Holstein theory calculations of trapped effective decay rates in the case of foreign-gas broadening. Consequently, the technique can be turned around so that measurements of effective radiative rates can yield unknown impact-regime line-broadening rates. A look at Eqs. (4) and (11) shows that while  $\Gamma_{\text{eff}} \propto (\Gamma_c/n)^{1/2}$ , the equivalent width  $W_\lambda \propto (\Gamma_c n)^{1/2}$ . Thus although measurements of  $W_\lambda$  and  $\Gamma_{\text{eff}}$  both suffer from random and systematic errors, their product is in-

dependent of sodium density which is a major source of uncertainty in the experiment. In fact, this product uniquely determines the broadening rate. Conversely, measurement of  $W_\lambda/\Gamma_{\text{eff}}$  can be used to obtain the radiating atom density even in situations where the broadening rate is unknown.

This situation is complicated by fine-structure mixing. From equations (4) and (11) it can be seen that

$$W_\lambda \Gamma_{\text{eff}} = 1.150 \frac{1}{2\pi c} \lambda^2 \Gamma_{\text{nat}} \Gamma_c \quad (13)$$

so that a plot of  $W_\lambda \Gamma_{\text{eff}}$  versus gas pressure gives a straight line whose slope yields the broadening constant  $k_c$ . In the complete mixing limit and at our temperatures, however, the measured decay rate  $\omega_-$  is given by  $0.342\Gamma_{1\text{eff}} + 0.658\Gamma_{2\text{eff}}$  and broadening rates for both lines become important. This can be disentangled by measuring equivalent widths on both lines and using Eq. (11) to show that

$$[W_\lambda(D_1)/W_\lambda(D_2)] = [\Gamma_c(D_1)/2\Gamma_c(D_2)]^{1/2}.$$

Substituting in, one can finally obtain

$$\Gamma_c(D_2) = \frac{1.14 \times 10^4 W_\lambda(D_2) \omega_-}{\left[1 + 1.04 \frac{W_\lambda(D_1)}{W_\lambda(D_2)}\right]}, \quad (14)$$

where the leading constant depends only on the transition wavelength, the speed of light, and the natural radiative rate (taken to be the same for both lines). The equivalent width is taken in angstroms. Figure 5 shows a plot of the right-hand side of Eq. (14) versus argon pressure for our sodium-argon data taken at 630 K. It can be seen that, within experimental uncertainties, the data are independent of Na density and that they can be fit by a straight line whose slope yields  $k_c^{\text{Ar}}(D_2) = (4.36 \pm 0.31) \times 10^{-9} \text{ cm}^3 \text{ s}^{-1}$ . In Table I we scale this result to 450 K and compare it to other measured values. From an expression similar to Eq. (14) for  $\Gamma_c(D_1)$ , we also obtain  $k_c^{\text{Ar}}(D_1) = (5.19 \pm 0.36) \times 10^{-9} \text{ cm}^3 \text{ s}^{-1}$ .

As a further demonstration of this technique we have measured sodium radiative decay rates  $\omega_-$  and absorption equivalent widths, versus noble-gas pressure in Na-Xe and Na-Ne mixtures. These results for the  $D_2$  line are also shown in Fig. 5. Broadening constants obtained from these and similar data are also listed in Table I where it can be seen that our results are in general agreement with previous results although our xenon results seem to be somewhat high. Our results are probably in best agreement with those of Kielkopf, but the uncertainties of our results are such that they should not be used to distinguish between the various published broadening rates. It can also be seen from the table that broadening rates obtained by different authors sometimes disagree by amounts greater than combined error bars. Somewhat more surprising is the disagreement between ratios of broadening constants obtained using different perturbing gases (see Table II). One would think that such ratios should be relatively free of systematic errors. At present, there is no explanation for these discrepancies other than that unidentified sources of error must exist in some of

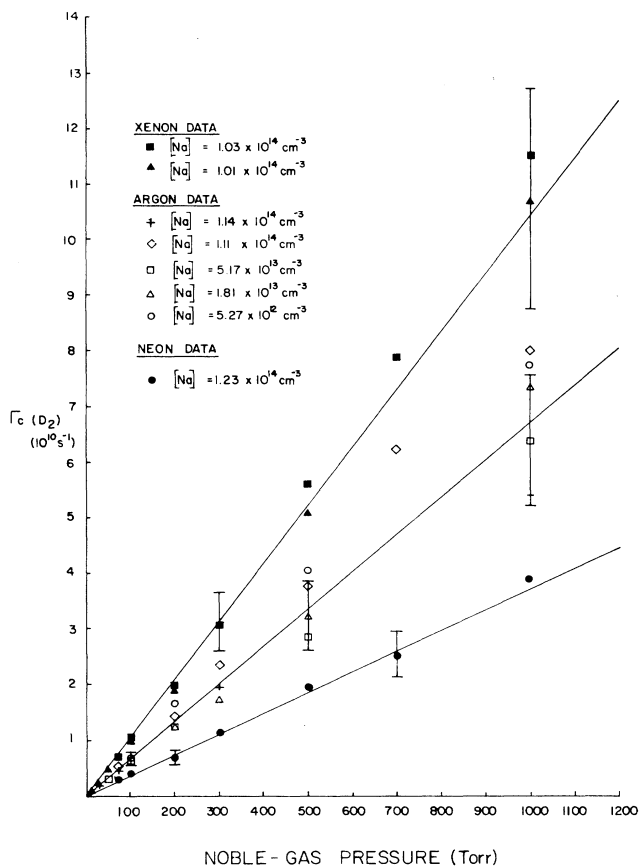


FIG. 5. Plot of the Na  $D_2$  line impact-regime collisional-broadening rates  $\Gamma_c(D_2)$ , vs noble-gas pressure.  $\Gamma_c(D_2)$  is obtained from Eq. (14). The broadening constants, obtained from the slopes of the least-squares straight line fits, are presented in Table I.

the experiments.

Because of these discrepancies in ratios of broadening rates, and in particular because of our very high value for  $k_c^{Xe}/k_c^{Ar}$ , we carried out one set of measurements of  $W_\lambda$  and  $\omega_-$  with fixed cell and reservoir temperatures, and 20–1000 Torr of either argon, neon, or xenon. Since these measurements were carried out on the same day and with all temperatures fixed, and since the xenon, argon and neon measurements were interwoven to avoid systematic effects, they should provide a sensitive test of the relative broadening rates. These results are given in parentheses in Table II. It can be seen that these values are more in line with the results of other experiments. Despite being based on a smaller number of points than the overall ratios, we believe these ratios in parentheses are the more accurate due to the canceling of systematic errors. We also report in Table II ratios of broadening rates derived solely from absorption equivalent widths measured during this final data run. These values agree well with those obtained from Eq. (14) and the equivalent  $D_1$  expression, verifying that the radiation trapping technique does not by itself introduce any serious systematic errors in these ratios of broadening rates.

It should be pointed out that, in general, our trapping measurements probe a region of the line shape further from line center than the earlier line-shape studies. Of course, our radiation trapping studies are not true line-shape studies at all, and the information we obtain is, in some sense, an average over the entire line. However, we are most sensitive to the part of the line where the optical depth is approximately unity. This point, of course, changes with gas pressure, but typically our broadening rates are mostly determined by the line profile at detunings of 1–50 GHz. The impact regime is defined by  $\Delta\omega \ll \tau_d^{-1}$  where  $\tau_d$  is the duration of a collision. For alkali-metal–noble-gas broadening,  $\tau_d^{-1}$  is typically 200 GHz. However, it is clear from the strong red asymmetry that we observe in our 1000-Torr xenon equivalent width absorption scans, that the quasistatic wings have some effect on our results, and this may be the main cause of the small but unaccounted discrepancies that exist between our results and those of other authors. These effects cannot be large, however, since they should manifest themselves by deviations from the square-root dependence of  $\omega_-$  on gas pressure (Fig. 4), and by deviations of the linear dependence of  $\Gamma_c$  on gas pressure (Fig. 5).

While determination of the broadening rates in our experiment does not require knowledge of the Na density, this information could be obtained from the ratios  $W_\lambda/\omega_-$ ; i.e.,

$$n = (2.21 \times 10^{20}) [W_\lambda(D_2)/\omega_-] \times \{1 + 1.04[W_\lambda(D_1)/W_\lambda(D_2)]\} \quad (15)$$

for our cell dimensions and temperature. Values of  $n$  obtained from this expression were self-consistent and agree with values from the Nesmayanov vapor pressure formula to within  $\sim 20\%$ .

Obviously we do not expect that this type of radiation trapping measurement will replace detailed line-shape studies. However, it does provide a quick and inexpensive method of measuring line broadening rates when no quenching takes place and when only 5–10% accuracy is required. Note that in the present experiment, temperature changes upon addition to the cell of foreign gas were fairly small (a few  $^\circ\text{C}$ ). However, this technique is immune to much larger temperature changes (that significantly alter the alkali-metal density) which sometimes plague line-shape studies. This is because the product  $W_\lambda\omega_-$  is independent of alkali-metal density, so long as  $W_\lambda$  and  $\omega_-$  are recorded under identical conditions. Conversely, the ratio  $W_\lambda/\omega_-$  can be used to track the alkali-metal density under such conditions. For example, in our data run where neon, argon, and xenon were used alternately to broaden the sodium lines, we found that neon caused an  $\sim 20\%$  increase, argon an  $\sim 10\%$  increase, and xenon no noticeable change in the sodium density. This is due to coupling of the side-arm reservoir temperature to the much hotter cell temperature by the gas, and to the fact that the thermal conductivity of neon is large, that of argon intermediate, and that of xenon quite small.

Recently, extensive theoretical and experimental studies of radiation trapping in mercury vapor have been carried out by Post<sup>19</sup> and Post *et al.*<sup>20</sup> This thorough work con-

TABLE I. Constants for broadening of the Na resonance lines by noble-gas perturbers (full width at half maximum) in units of  $10^{-9} \text{ rad s}^{-1} \text{ cm}^3$ .

		Reference	$T$ (K)	$k_c(D_1)$	$k_c(D_2)$	Results scaled to 450 K		$k_c(D_1)/k_c(D_2)$	
						$k_c(D_1)$	$k_c(D_2)$		
Argon	Expt.	This work	630	$5.19 \pm 0.36$	$4.36 \pm 0.31$	$4.69 \pm 0.33^a$	$3.94 \pm 0.28^a$	1.19	
		11	475	$5.54 \pm 0.40$	$4.54 \pm 0.40$	$5.45 \pm 0.40$	$4.47 \pm 0.40$	1.22	
		12	450	$4.86 \pm 0.04$	$4.45 \pm 0.11$	$4.86 \pm 0.04$	$4.45 \pm 0.11$	1.09	
		13 <sup>b</sup>	450	$5.56 \pm 0.28$	$4.22 \pm 0.21$	$5.56 \pm 0.28$	$4.22 \pm 0.21$	1.32	
		14	410	$4.13 \pm 0.27$	$4.11 \pm 0.26$	$4.25 \pm 0.28$	$4.23 \pm 0.27$	1.00	
		15	360	$4.49 \pm 0.12$	$4.14 \pm 0.14$	$4.80 \pm 0.13$	$4.43 \pm 0.14$	1.08	
	Theory	35,36	450	4.96	4.28	4.96	4.28	1.16	
	Xenon	Expt.	This work	630	$7.45 \pm 0.52$	$6.78 \pm 0.47$	$6.73 \pm 0.47^a$	$6.13 \pm 0.42^a$	1.10
			11	475	$5.26 \pm 0.41$	$4.64 \pm 0.47$	$5.18 \pm 0.40$	$4.57 \pm 0.46$	1.13
			12	450	$5.96 \pm 0.26$	$5.73 \pm 0.19$	$5.96 \pm 0.26$	$5.73 \pm 0.19$	1.04
13 <sup>b</sup>			450	$5.83 \pm 0.29$	$4.94 \pm 0.25$	$5.83 \pm 0.29$	$4.94 \pm 0.25$	1.18	
14			410	$4.77 \pm 0.31$	$4.85 \pm 0.32$	$4.91 \pm 0.32$	$4.99 \pm 0.33$	0.98	
15			360	$5.54 \pm 0.16$	$5.07 \pm 0.16$	$5.92 \pm 0.17$	$5.42 \pm 0.17$	1.09	
Theory		35,36	4.50	7.14	5.86	7.14	5.86	1.22	
Neon		Expt.	This work	630	$2.04 \pm 0.22$	$2.40 \pm 0.23$	$1.78 \pm 0.19^c$	$2.10 \pm 0.20^c$	0.85
			11	475	$2.82 \pm 0.20$	$2.88 \pm 0.20$	$2.76 \pm 0.20$	$2.82 \pm 0.20$	0.98
			12	450	$1.91 \pm 0.05$	$2.13 \pm 0.35$	$1.91 \pm 0.05$	$2.13 \pm 0.35$	0.90
	13 <sup>b</sup>		450	$2.79 \pm 0.14$	$2.53 \pm 0.13$	$2.79 \pm 0.14$	$2.53 \pm 0.13$	1.10	
	14		410	$2.17 \pm 0.14$	$2.26 \pm 0.15$	$2.25 \pm 0.15$	$2.35 \pm 0.16$	0.96	
	15		360	$1.86 \pm 0.06$	$2.04 \pm 0.08$	$2.03 \pm 0.07$	$2.23 \pm 0.09$	0.91	
	Theory	35,36	450	2.98	3.10	2.98	3.10	0.96	

<sup>a</sup>The argon and xenon results have been scaled to 450 K using the observed  $T^{0.3}$  temperature dependence (Ref. 36). This result is in agreement with the theoretical temperature dependence predicted for van der Waals broadening.

<sup>b</sup>Published uncertainties have been revised to 5% (Ref. 37).

<sup>c</sup>The neon results have been scaled to 450 K using the observed  $T^{0.4}$  temperature dependence (Ref. 36). This result is intermediate between the theoretical temperature dependence predicted for van der Waals broadening ( $T^{0.3}$ ), and that for hard-sphere broadening ( $T^{0.5}$ ).

TABLE II. Ratios of broadening constants. Due to the different temperature dependences of the neon and argon broadening constants, the ratios reported in columns 3 and 4 are valid only at 450 K.

Reference	$k_c^{\text{Xe}}(D_1)/k_c^{\text{Ar}}(D_1)$	$k_c^{\text{Xe}}(D_2)/k_c^{\text{Ar}}(D_2)$	$k_c^{\text{Ne}}(D_1)/k_c^{\text{Ar}}(D_1)$	$k_c^{\text{Ne}}(D_2)/k_c^{\text{Ar}}(D_2)$
Experiment				
This work	1.44 (1.31) <sup>a</sup>	1.56 (1.38) <sup>a</sup>	0.380 (0.325) <sup>a</sup>	0.533 (0.449) <sup>a</sup>
Equivalent width (this work)	1.24	1.34	0.382	0.509
McCartan and Farr (Ref. 11)	0.95	1.02	0.506	0.631
Kielkopf (Ref. 12)	1.23	1.29	0.393	0.479
Chatham <i>et al.</i> (Ref. 13)	1.05	1.17	0.502	0.600
Kachru <i>et al.</i> (Ref. 14)	1.15	1.18	0.529	0.556
Walkup <i>et al.</i> (Ref. 15)	1.23	1.22	0.423	0.503
Theory				
Lwin <i>et al.</i> (Refs. 35 and 36)	1.44	1.37	0.601	0.724

<sup>a</sup>Numbers in parentheses represent broadening rate ratios taken on the same day, with all temperatures fixed, and with argon, xenon, and neon data interwoven to avoid systematic effects.

siders the effects of hyperfine structure and demonstrates the important influence of incomplete frequency redistribution under certain conditions. This latter effect was previously considered in some detail by Payne *et al.*<sup>38</sup> We consider our present work to be complementary to the work of Post *et al.* In our experiment, we have endeavored to study radiation trapping in the simplest possible environment where natural broadening can be neglected, where the broadening and collisional excitation transfer rates are well known, and where the ground state atom density is uniform over a nearly ideal geometry. Post *et al.* carried out their experiments in a discharge where nonuniform absorbing atom densities and temperatures and the complications of charged particles had to be sorted out. The good agreement found between measured and calculated decay rates under their conditions demonstrates that their theoretical formulation of the radiation trapping problem with incomplete redistribution is fundamentally correct. The analytic expressions for the effective radiative rate developed by Post contain fewer approximations than Holstein's formulation and thus are not as simple or easy to use as the Holstein expressions. However, we note that the expressions of Post agree with those of Holstein<sup>6,7</sup> and van Trigt<sup>8,9</sup> in the limit of complete redistribution and a line with only one hyperfine structure component. Streater *et al.*<sup>21,39</sup> have also recently developed a theory of trapping including incomplete redistribution, which improves upon previous work by correctly accounting for the instantaneous nature of Rayleigh scattering. This difference between the Streater and Post theories will only manifest itself on a time scale comparable to or smaller than the natural lifetime,<sup>40</sup> and thus while it is important in many applications, it would not be observable in experiments such as those presented here or in Refs. 19 and 20. We should finally note that in comparing the Holstein theory to experiment in the natural broadening limit, it is not justified to simply add  $\Gamma_{\text{nat}}$  to  $\Gamma_c$  in Eq. (4). Since  $\Gamma_{\text{nat}}$  does not redistribute the photon frequency, and Rayleigh scattering produced by the natural wings is effectively instantaneous, a more accurate approximation is simply to ignore natural broadening and use whichever of the Doppler or pressure broadening formulas [(3) or (4)] as yields the largest value for  $\Gamma_{\text{eff}}$ . We have shown here and in Ref. 10 that this empirical ap-

proach yields accurate values for  $\Gamma_{\text{eff}}$  as long as the density range where natural broadening dominates the trapping problem is not too large. The criteria for determining where natural broadening can be ignored has been discussed at length by Payne *et al.*<sup>38</sup> However, in the case where natural broadening cannot be ignored, the theoretical development of Post<sup>19</sup> and Streater *et al.*<sup>21,39</sup> appears to accurately handle the trapping problem, allowing calculation of fundamental-mode decay rates.

#### IV. CONCLUSIONS

In summary, we have tested the Holstein theory of radiation trapping for resonance lines broadened by foreign gas (van der Waals broadening). The results show that the theory yields accurate values for effective radiative decay rates when the validity criteria of the theory are satisfied, and thus enables experimenters to calculate  $\Gamma_{\text{eff}}$  quickly and accurately under a wide range of experimental conditions. This is especially important to those who wish to use cw laser techniques to determine rate coefficients for collision processes that compete with radiative decay.

We have also demonstrated that confirmation of the Holstein theory allows a simple technique for measuring impact-regime pressure broadening rates with reasonable accuracy. This technique is valid only for resonance lines and in the absence of quenching collisions. However, fine-structure mixing is handled by the technique and broadening rates for individual fine-structure levels are obtained.

#### ACKNOWLEDGMENTS

The authors would like to thank Dr. Will Happer of Princeton for the generous loan of several key pieces of equipment and Dr. Alan Gallagher, Dr. Linda Vahala, and Dr. Jinx Cooper for useful discussions. We would also like thank Dr. Yong Kim for the use of a pulsed dye laser system during the early stages of this experiment and to acknowledge financial support of this work from the Research Corporation, the Energy Research Center at Lehigh University, the National Science Foundation under Grant No. PHY-8451279, and GTE Laboratories Inc.

\*Present address: Department of Physics, Massachusetts Institute of Technology, Cambridge, MA 02139.

†Present address: Department of Physics, Cornell University, Ithaca, NY 14853.

<sup>1</sup>D. Mihalas, *Stellar Atmospheres* (Freeman, San Francisco, 1970).

<sup>2</sup>J. Huennkens and A. Gallagher, *Phys. Rev. A* **27**, 771 (1983).

<sup>3</sup>J. Huennkens and A. Gallagher, *Phys. Rev. A* **27**, 1851 (1983).

<sup>4</sup>J. Maya, M. W. Grossman, R. Lagushenko, and J. F. Waymouth, *Science* **226**, 435 (1984).

<sup>5</sup>J. B. Anderson, J. Maya, M. W. Grossman, R. Lagushenko, and J. F. Waymouth, *Phys. Rev. A* **31**, 2968 (1985).

<sup>6</sup>T. Holstein, *Phys. Rev.* **72**, 1212 (1947).

<sup>7</sup>T. Holstein, *Phys. Rev.* **83**, 1159 (1951).

<sup>8</sup>C. van Trigt, *Phys. Rev.* **181**, 97 (1969).

<sup>9</sup>C. van Trigt, *Phys. Rev. A* **13**, 726 (1976).

<sup>10</sup>J. Huennkens and A. Gallagher, *Phys. Rev. A* **28**, 238 (1983).

<sup>11</sup>D. G. McCartan and J. M. Farr, *J. Phys. B* **9**, 985 (1976).

<sup>12</sup>J. F. Kielkopf, *J. Phys. B* **13**, 3813 (1980).

<sup>13</sup>R. H. Chatham, A. Gallagher, and E. L. Lewis, *J. Phys. B* **13**, L7 (1980).

<sup>14</sup>R. Kachru, T. W. Mossberg, and S. R. Hartmann, *J. Phys. B* **13**, L363 (1980).

<sup>15</sup>R. Walkup, A. Spielfiedel, D. Ely, W. D. Phillips, and D. E. Pritchard, *J. Phys. B* **14**, 1953 (1981).

<sup>16</sup>J. Pitre and L. Krause, *Can. J. Phys.* **45**, 2671 (1967).

<sup>17</sup>R. Seiwert, *Ann. Phys. (Leipzig)* **18**, 54 (1956).

<sup>18</sup>G. Copley, B. P. Kibble, and L. Krause, *Phys. Rev.* **163**, 34

- (1967).
- <sup>19</sup>H. A. Post, *Phys. Rev. A* **33**, 2003 (1986).
- <sup>20</sup>H. A. Post, P. van de Weijer, and R. M. M. Cremers, *Phys. Rev. A* **33**, 2017 (1986).
- <sup>21</sup>A. Streater, Ph.D. thesis, University of Colorado, 1985.
- <sup>22</sup>A. Corney, *Atomic and Laser Spectroscopy* (Clarendon, Oxford, 1977).
- <sup>23</sup>W. L. Wiese, M. W. Smith, and B. M. Miles, *Atomic Transition Probabilities*, Natl. Stand. Ref. Data Ser., Natl. Bur. Stand. (U.S.) Circ. No. 22 (U.S. GPO, Washington, D.C., 1969), Vol. II.
- <sup>24</sup>A. N. Nesmayanov, *Vapor Pressure of the Elements* (Academic, New York, 1963).
- <sup>25</sup>Equivalent width program VPROF written by C. Kunasz and W. Kamke.
- <sup>26</sup>A. C. G. Mitchell and M. W. Zemansky, *Resonance Radiation and Excited Atoms* (Cambridge University Press, Cambridge, 1934).
- <sup>27</sup>L. K. Lam, T. Fujimoto, and A. C. Gallagher, *J. Chem. Phys.* **68**, 3553 (1978).
- <sup>28</sup>L. H. Aller, *Astrophysics—The Atmospheres of the Sun and Stars* (Ronald, New York, 1953).
- <sup>29</sup>S. Tsuchiya and K. Kuratani, *Combust. Flame* **8**, 299 (1964).
- <sup>30</sup>J. H. Stamper, *J. Chem. Phys.* **43**, 759 (1965).
- <sup>31</sup>W. Demtroder, *Z. Phys.* **166**, 42 (1962).
- <sup>32</sup>B. P. Kibble, G. Copley, and L. Krause, *Phys. Rev.* **159**, 11 (1967).
- <sup>33</sup>G. W. Norrish and W. M. Smith, *Proc. R. Soc. London, Ser. A* **176**, 295 (1941).
- <sup>34</sup>I. Tanarro, F. Arqueros, and J. Campos, *J. Chem. Phys.* **77**, 1826 (1982).
- <sup>35</sup>N. Lwin, D. G. McCartan, and E. L. Lewis, *J. Phys. B* **9**, L161 (1976).
- <sup>36</sup>N. Lwin, D. G. McCartan, and E. L. Lewis, *Astrophys. J.* **213**, 599 (1977).
- <sup>37</sup>A. Gallagher and E. L. Lewis (private communication).
- <sup>38</sup>M. G. Payne, J. E. Talmage, G. S. Hurst, and E. B. Wagner, *Phys. Rev. A* **9**, 1050 (1974).
- <sup>39</sup>A. Streater, J. Cooper, and W. Sandle (unpublished).
- <sup>40</sup>J. Cooper (private communication).